

Stochastic Modeling of the Independent Roles of Particle Size and Grain Size in Transgranular Cleavage Fracture

TSANN LIN, A. G. EVANS, and R. O. RITCHIE

The independent roles of grain size and particle size on sharp crack and rounded notch toughness are investigated over a range of temperatures from the lower shelf into the early ductile/brittle transition region. The results are interpreted in terms of a weakest link statistical model wherein the onset of failure coincides with the critical propagation of a particle microcrack into the matrix. It is shown that, for a fixed particle size distribution, both sharp-crack and rounded-notch toughness decrease with increasing grain size. However, at fixed grain size, the sharp-crack toughness increases, while the rounded-notch toughness decreases with increasing particle size. Such effects result primarily from the difference in the number of activated particles in the plastic zone.

I. INTRODUCTION

CLEAVAGE fracture in most metals occurs by the nucleation of a microcrack, assisted by the local plastic deformation of the surrounding material, and its continued propagation when the local, concentrated, tensile stress exceeds some critical fracture stress. In mild steels, such microcracks were originally considered to nucleate at grain boundaries, which act as barriers to slip-bands.^{1,2,3} Consequently, since the grain size determines the dislocation pile-up length, as well as the distance to the first crack extension barrier (*i.e.*, the next grain boundary), early models of cleavage fracture identified the grain size as the sole, dominant microstructural feature.^{1,2,3} Later studies⁴⁻⁷ associated the microcracks with the fracture of grain boundary carbide particles. Thus, particle size emerged as an additional key microstructural feature.

The relative importance of particle size and grain size is also, in part, dependent on the critical step in the cleavage process. When the critical event involves the continued propagation of the particle microcrack into the matrix, the particle size is clearly the salient dimension (aside from the indirect effect of grain size on yield strength), consistent with the majority of microstructural observations on failure at very low temperatures on the lower toughness shelf. At somewhat higher temperatures, approaching the ductile/brittle transition region, observations of grain size microcracks suggest that the critical step involves consideration of dynamic propagation and arrest at the next grain boundary, a mechanism favoring grain size as the salient dimension.

Most heat treatments change *both* microstructural dimensions. Consequently, there have been few attempts⁸ to investigate the separate roles of particle size and grain size. The objective of the present work is to examine this issue. For this purpose, a recently developed statistical model for

cleavage fracture at low temperatures^{9,10} will be used in conjunction with experiments on simple ferrite/grain boundary carbide microstructures, for which the particle and grain sizes have been varied independently.

II. MECHANISMS OF CLEAVAGE FRACTURE

The process of cleavage fracture in steels seemingly involves three critical steps: crack nucleation at carbide particles, crack propagation across the carbide/ferrite interface, and crack propagation across the first ferrite/ferrite grain boundary.^{5,6,12} The conditions that dominate each of these processes typically vary with microstructure and with temperature. However, none of these processes is sufficiently well-quantified that the prediction of trends can be made *a priori*. Nevertheless, a general discussion of the processes involved provides a framework suitable for the interpretation of cleavage fracture observations and measurements.

A. Crack Nucleation

Substantial experimental evidence suggests that the nucleation of cracks occurs in carbide particles and requires some plastic deformation of the ferrite.⁵⁻²⁰ Indeed, cracked carbides have only been identified quite close to the crack, well within the plastic zone,^{7,10,11} indicating that *significant plastic strain* is needed to achieve nucleation. Thus, while dislocation pile-up arguments for crack nucleation are conceptually attractive, a continuum plasticity analysis may often be more pertinent.* Such analysis indicates that the

*Continuum results become appropriate when the slip band spacing is significantly smaller than the particle size.

maximum principal tensile stress in the *particle* is given by:

$$\sigma_{11} = \sigma_m + \lambda \bar{\sigma} \quad [1]$$

where σ_m is the mean stress and $\bar{\sigma}$ is the equivalent stress in the matrix and λ is a coefficient of order 2.²¹ For a power hardening solid, the constitutive law, given in terms of the work hardening exponent n and yield stress and strain, σ_0 and ϵ_0 , respectively, is ($\bar{\epsilon} \geq \epsilon_0$):

$$\bar{\sigma} = \sigma_0 (\bar{\epsilon} / \epsilon_0)^{1/n} \quad [2]$$

Hence, under small-scale yielding, the stress distribution, as a function of distance r ahead of the crack tip, is given by the Hutchinson-Rice-Rosengren (HRR) nonlinear elastic singular field.^{22,23}

TSANN LIN, formerly Graduate Student in the Department of Materials Science and Mineral Engineering, University of California, Berkeley, is with IBM Corporation, Yorktown Heights, NY. A. G. EVANS is Professor, Materials Program, University of California, Santa Barbara, CA 93106. R. O. RITCHIE is Professor, Materials and Molecular Research Division, Lawrence Berkeley Laboratory, and Department of Materials Science and Mineral Engineering, University of California, Berkeley, CA 94720.

This paper is based on a presentation made at the symposium "Stochastic Aspects of Fracture" held at the 1986 annual AIME meeting in New Orleans, LA, on March 2-6, 1986, under the auspices of the ASM/MSD Flow and Fracture Committee.

$$\sigma_{ij} = \sigma_0 \left(\frac{J}{\sigma_0 \epsilon_0 I_n r} \right)^{1/(n+1)} \bar{\sigma}_{ij}(\theta) \quad [3]$$

where J is the path-independent integral. Crack nucleation can thus be predicted to occur within a zone bounded by:

$$r_N^* = \left(\frac{J}{\sigma_0 \epsilon_0 I_n} \right) \left(\frac{\sigma_0}{\sigma_c} \right)^{n+1} \frac{1}{(\bar{\sigma}_m + \lambda \bar{\sigma})^{n+1}}, \quad (r > 2\delta) \quad [4]$$

where σ_c is the critical stress needed to crack the particle, and I_n and $\bar{\sigma}_{ij}$ are dimensionless functions in the HRR solution (tabulated in Reference 24). Typically, σ_c would be expected to have appreciable statistical variability, giving rise to a corresponding range in r_N^* .

The preceding considerations do not explicitly involve either the particle size or the grain size. However, these dimensions have indirect involvement by virtue of statistical size effects on the critical cracking stress, σ_c , and the effects of grain size on the flow stress. Observations of stable, cracked carbides in the plastic zone suggest that crack nucleation is not normally the critical step. However, situations wherein nucleation is the dominant step cannot be precluded, as discussed below.

B. Particle Cracks

Dynamic crack propagation within the carbide, subject to Eq. [3], is unlikely to activate significant plastic deformation in the ferrite, because the predominant shear field is within the particle (Figure 1). The cleavage crack may thus extend dynamically across the interface, provided that the stress σ_{11} exceeds the effective particle strength S , given in terms of the particle size d_p , by:⁷

$$S = [\pi E G_{cf} / 2(1 - \nu^2) d_p]^{1/2} \quad (\text{penny-shaped crack}) \quad [5]$$

where E is Young's modulus, ν is Poisson's ratio, and G_{cf} is the critical strain energy release rate for *dynamic* propa-

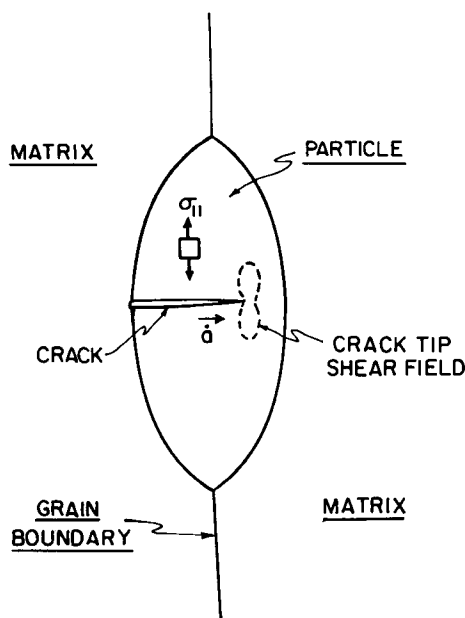


Fig. 1—Illustration of possible critical steps in nucleation- and propagation-controlled cleavage fracture, involving, respectively, microcrack formation in a grain boundary carbide and its propagation into the surrounding matrix.

gation of a crack into the ferrite matrix (which, it is recalled, has previously experienced significant plastic strain).

Should S be larger than σ_{11} (by virtue of a small particle size), the crack would arrest at the interface. Results described below, and elsewhere,²⁵ suggest that, when the crack arrests, crack blunting ensues and subsequent propagation of the particle crack is essentially excluded. Indeed, *observations* of quasi-static crack extension from a brittle solid (Al_2O_3) into a bcc metal (Nb) reveal that the crack blunts and arrests at the interface (Figure 2), whereas rapidly moving cracks extend unstably with little attendant plasticity.²⁶ Furthermore, *calculations* of dynamic crack propagation in body-centered cubic (bcc) metals indicate that the plastic zone shrinks as the crack velocity increases,²⁷ causing a substantial reduction in G_{cf} with increase in crack velocity. This duality, indicated schematically in Figure 2, supports the notion that cleavage crack extension from the carbide into the ferrite is necessarily a dynamic process. Moreover, the experimental evidence, that G_{cf} is in the range 30 to 50 Jm^{-2} (e.g., Reference 28), constitutes a reasonable estimate for the expected dynamic fracture resistance of the ferrite. Consequently, the first carbide particle that satisfies both the nucleation requirement and the above propagation requirement becomes the fracture critical entity. Particles that nucleate cracks, but are too small to satisfy the propagation criterion, would contain stable cracks that may act as subsequent nuclei for void growth when ductile fracture intervenes.

The preceding description of cleavage fracture satisfies, in statistical terms, the weakest link requirements. However, the population being sampled may be a function of plastic strain, and hence distance from the crack tip, within the plastic zone. With this restriction, weakest link concepts can give the failure criterion,^{9,16-20} with the particle strength S , given by Eq. [5], being the pertinent "strength" distribution.^{9,16,19} However, it is further noted that, since the crack

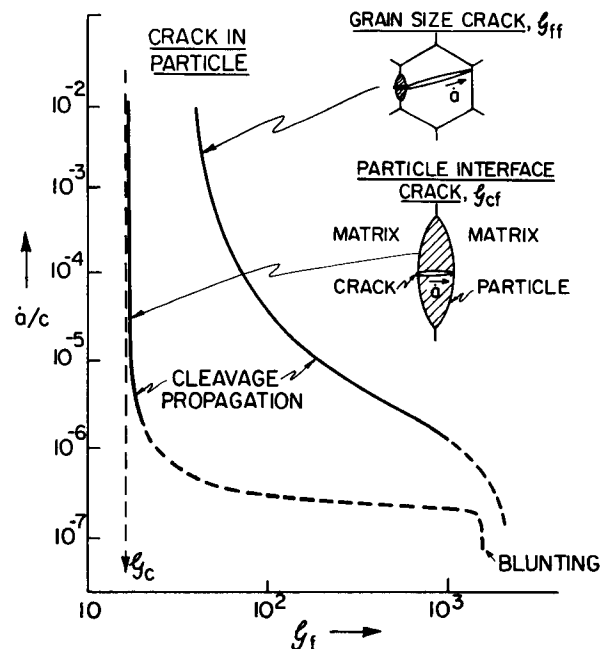


Fig. 2—Schematic representation of the variation in the dynamic strain energy release rate (effective fracture energy) with crack velocity \dot{a} for the propagation of a cleavage crack originating from the critical extension of either a microcrack in the particle interface or a grain-size microcrack.

emanating from the particle is not likely to activate much plasticity in the matrix, the magnitude of the dynamic G_{cf} , and hence, of S , is likely to be relatively insensitive to temperature, as indicated in Figure 3.

C. Ferrite/Ferrite Cracking

Crack extension into the ferrite is undoubtedly accompanied by a plastic zone (Figure 4). The dynamic critical strain energy release rate, G_{ff} , at the first ferrite/ferrite interface is thus expected to exceed appreciably that of the carbide/ferrite interface (Figure 2). Furthermore, effects of rate (Figure 2) and of temperature on G_{ff} are expected to be greater.

Continued dynamic extension of the crack across the ferrite/ferrite boundary occurs when the stress exceeds the "ferrite grain strength", given in terms of the grain diameter d_g by:

$$\Sigma = [\pi E G_{ff} / (1 - \nu^2) d_g]^{1/2} \quad [6]$$

Comparison with Eq. [5] indicates that:

$$\Sigma/S = (d_p G_{ff} / d_g G_{cf})^{1/2} \quad [7]$$

When $\Sigma < S$, the microcrack would not normally arrest at the ferrite grain boundary, and unstable cleavage fracture

would ensue from particle cracking. However, the condition $\Sigma > S$ allows crack arrest, resulting in the appearance of stable, grain-sized microcracks.*

*Equations [5] and [6] are small scale yielding solutions for dynamic cleavage crack extension across the carbide/ferrite interface and the ferrite grain boundary, respectively. Small scale yielding results are deemed appropriate, despite the prior quasi-static plastic deformation of the grains, because the cleavage cracks that continue across the barrier and cause fracture are dynamic, whereupon the associated *dynamic* plastic zone that dictates G_{cf} and G_{ff} is expected to satisfy small scale yielding requirements (see Figures 1 and 4) and thereby, be in accordance with the predictions of Hutchinson and Freund.²⁷

With the premise that G_{ff} has a stronger temperature dependence than G_{cf} (because of the stronger influence of plasticity (Figures 1 and 4)), a transition could be expected. Specifically, since $d_p \ll d_g$, S is likely to exceed Σ at low temperature. However, at higher temperatures, because of the anticipated rapid increase in G_{ff} , a transition to $\Sigma > S$ would occur. This behavior is summarized on Figure 3, indicating the region in which stable grain-size microcracks would be expected.

D. Fracture Trends

The effects of temperature on fracture behavior can be conveniently summarized in a stress/temperature diagram (Figure 3), containing the expected temperature dependence of the yield strength, σ_0 , the peak stress in the plastic zone, $\hat{\sigma}$, as well as the particle "strength" S and matrix grain "strength" Σ . Such a diagram identifies the regions of nucleation and propagation control in the cleavage domain, plus particle/matrix interface and matrix/matrix interface limited behavior in the propagation dominated domain.

The various regions of behavior are dictated by the respective stress levels. At the lowest temperature, both S and Σ are below the yield strength* and hence, cleavage

*Note that strain-rate sensitivity in the cleavage fracture and transition processes arise because of the strain rate sensitivity of σ_0 .

fracture occurs once nucleation condition is satisfied, in accordance with Eq. [4]. *Nucleation* dominated behavior would then pertain. At higher temperatures, S exceeds both the yield strength and Σ , but is less than the peak stress, $\hat{\sigma}$. The particles would thus crack, without causing failure. Particles which satisfy the dynamic criterion for propagation across the particle/matrix interface ($\sigma_{11} > S$, Eq. [5]), would then become the source of cleavage fracture. At still higher temperatures, both S and Σ exceed the yield strength, but $\Sigma > S$. Hence, particles may crack and the crack can extend to the first ferrite grain boundary without causing failure. Stable grain size cracks would then become possible. In this temperature range, cleavage fracture would occur when a crack can extend dynamically across the ferrite grain boundary, in accordance with the condition that the average stress on the grain $\sigma > \Sigma$. Finally, at the highest temperature, the peak stress in the plastic zone, $\hat{\sigma}$, becomes less than both S and Σ . Cleavage fracture is then impossible and the transition to ductile fracture occurs.*

*However, particle cracking can still occur above the transition temperature. These blunted cracks are stable, but may act as nuclei for the voids which ultimately cause ductile fracture.

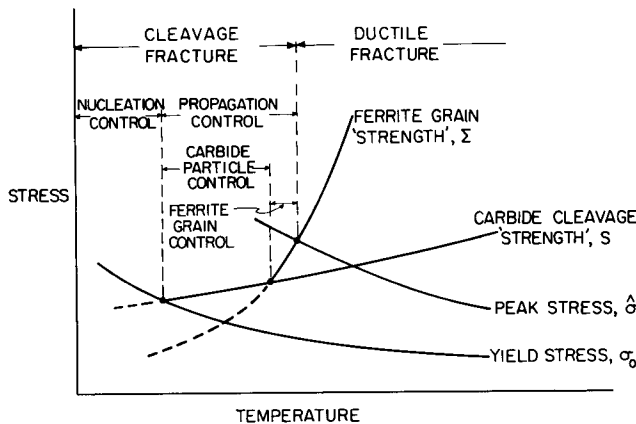


Fig. 3—Schematic representation of the variation with temperature of the cleavage fracture "strength", resulting from either particle microcracks or grain-size microcracks, indicating the regions of nucleation- and propagation-control.

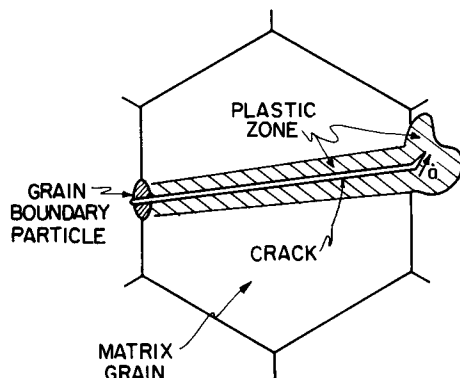


Fig. 4—Illustration of an alternative critical step in propagation-controlled cleavage fracture, involving the propagation of a grain-size microcrack through the next grain boundary.

III. WEAKEST LINK MODELS

When the critical cleavage fracture step is the propagation of the particle microcracks into the matrix grains (Figure 3), fracture can be analyzed using weakest link statistics.^{9,10,16-20} For this purpose, the plastic zone is divided into constant tensile stress elemental volumes, dV , all of which must "survive" to avoid cleavage fracture. Using the weakest-link assumption, the total survival probability of the entire structure can be stated as the product of the survival probabilities of all elements:²⁹

$$\Phi = 1 - \exp\left\{-\int_0^V \left[dV \int_0^\sigma g(S) dS \right]\right\} \quad [8]$$

where V is the plastic zone volume, and $g(S)dS$ is the number of cracked particles, per unit volume, having strengths between S and $S + dS$. A convenient and versatile expression for $g(S)dS$ is the three-parameter Weibull expression:³⁰

$$\int_0^\sigma g(S) dS = \left[\frac{\sigma - S_u}{S_0} \right]^m fN_0, \quad [9]$$

where m is a shape factor, S_0 is a scale parameter, S_u is a lower bound strength (of the largest feasible particle), N_0 is the number of particles per unit volume, and f represents the fraction of "eligible" particles that participate in the fracture process. Eligibility is determined by the requirements that both the crack nucleation and crack propagation requirements be satisfied, as discussed in Section II. Given the stress field within the plastic zone (considered in the present model in terms of the maximum principal stress), the toughness can be estimated in terms of the volume of material needed to assure the presence of an "eligible" particle. Furthermore, the scatter in toughness values can be related to the particle size distribution.

Since the probability of finding an "eligible" particle is promoted with increasing volume, *i.e.*, with increasing distance from the tip, the site of the critical fracture event depends primarily upon whether the local stress gradient (over the relevant microstructural size-scale) is negative, as in the case of a sharp crack, or positive, as in the case of a rounded notch.¹⁰

For fracture ahead of a *sharp crack*, there is a competition between behavior away from the tip, where the population of eligible particles is large, but stresses are low, and behavior close to the tip, where stresses are higher but the number of eligible particles is small. Consequently, the critical fracture event is located at some intermediate distance within the plastic zone, where the elemental failure probability exhibits a maximum.^{9,10} At low temperatures (where $S \approx \sigma_0$), fracture is dominated by the region close to the elastic/plastic interface, resulting in the site of maximum fracture probability:

$$r_f^* = \frac{(5 - m)^2}{50\pi} \left(\frac{K_{Ic}}{S_u} \right)^2, \quad [10a]$$

where r_f^* is the so-called characteristic distance (generally of the order of a few grain diameters¹⁰). At higher temperatures, where fracture is dominated by the nonlinear HRR stress field,^{22,23} the analogous result is:

$$r_f^* = \tilde{\sigma}^{n+1} \left(\frac{1 - \nu^2}{I_n} \right) \left(\frac{2n + 3 - m}{2n + 3} \right)^{n+1} \left(\frac{\sigma_0}{S_u} \right)^{n+1} \left(\frac{K_{Ic}}{\sigma_0} \right)^2 \quad [10b]$$

where K_{Ic} is the fracture toughness.⁹ The magnitude of K_{Ic} , evaluated at the median level ($\Phi = 0.5$), is then given by:⁹

$$K_{Ic} = \left(\frac{\ln 2}{1.35\eta f N_0 b} \right)^{1/4} \left(\frac{S_0}{S_u} \right)^{m/4} S_u \quad [11a]$$

at low temperature, and:

$$K_{Ic} = \left(\frac{\ln 2}{\xi \eta f N_0 b} \right)^{1/4} \left(\frac{S_0}{S_u} \right)^{m/4} S_u^{(1+n)/2} \sigma_0^{(1-n)/2} \quad [11b]$$

at higher temperature,* where b is a characteristic di-

*Strain-rate sensitivity of K_{Ic} in this temperature region is associated with the strain-rate dependence of σ_0 .

mension describing the distance between initial nucleation events along the crack front,¹⁹ and ξ and η are functions of I_n , n , S , S_u , and $\tilde{\sigma}$, evaluated in Reference 9. The low temperature solution (Eq. [11a]) provides a temperature-independent K_{Ic} asymptote (lower shelf), whereas the nonlinear solution (Eq. [11b]) becomes asymptotic to a transition temperature.⁹

For cleavage ahead of a *rounded notch*, the corresponding stress fields have a shallower (positive) gradient.^{31,32} Consequently, the local stress and the probability of finding an "eligible" particle *both* increase with increasing distance from the notch, within the plastic zone. Statistically, there is now less competition between the location of the eligible crack nuclei and the highest stresses, with the result that the critical event occurs far from the notch root, close to the elastic-plastic interface.¹⁰ For a non-hardening solid, the characteristic distance from the notch root where the initial cracking event is most probable is given by:¹⁰

$$r_f^* = \rho \exp\left\{ \frac{1}{4} \left[(\pi - 4\zeta - 2) - 2(m + s) + \sqrt{(\pi - 4\zeta - 2)^2 + 4(m + s)^2 + 8m} \right] \right\} \quad [12]$$

where ρ is the notch root radius, ζ describes the boundary of the slip-line field, and s is given by $[1 - (\sqrt{3}/2)(S_u/\sigma_0)]$. Similar expressions can be developed for power hardening solids,¹⁰ but are too unwieldy to be presented here. The total failure probability, however, can be expressed as:¹⁰

$$\Phi = 1 - \exp\left[-fN_0 b \int_\rho^{r_f^*} \left(\frac{\sigma_0 D_1 D_2 - S_u}{S_0} \right)^m \times \left(\pi - 4\zeta - 2 \ln \frac{r}{\rho} \right) r dr \right] \quad [13]$$

where D_1 is a function of n , σ_0/E , and the strain at the notch root, and D_2 is a function of n and r/ρ . Both functions are evaluated in Reference 10. Analogous to the predictions of K_{Ic} for a sharp crack (Eq. [11]), the above equations can

be used to predict the fracture load for failure ahead of a rounded notch.¹⁰

IV. EXPERIMENTAL PROCEDURES

The material used for the present study was an AISI 1008 mild steel, of composition shown in Table I.

The steel was heat treated to give ferritic microstructures with predominately grain-boundary carbides. To vary the carbide and ferrite grain size independently, specimens were austenitized at either 920 °C or 1200 °C, air cooled, and then spheroidized at 700 °C for either 3 or 7 days. Grain size was varied by austenitization treatment. A fine-grained structure (termed L), with a 25 μm average ferritic grain size, was obtained following 1 hour at 920 °C, and a coarser-grained structure (termed H), with average size 45 μm , by austenitizing for 1 hour at 1200 °C. Conversely, carbide size was varied by spheroidization, following 3 and 7 day tempering treatments (termed 3 and 7, respectively). Reference tests were performed on a 920 °C austenitized structure, spheroidized for 30 days in order to generate an extremely coarse distribution of carbides (termed L30).

Particle size distributions (Figure 5) were determined by counting carbides according to their areas, using a quantitative image analyzer. Mechanical properties were assessed from uniaxial tensile tests conducted at an initial strain rate of $3 \times 10^{-4} \text{ s}^{-1}$ over the temperature range $-196 \text{ }^\circ\text{C}$ to 20 °C. Plane strain fracture toughness, K_{Ic} , was evaluated on fatigue precracked single-edge-notched (SEN) specimens, tested in four-point bending over the temperature range, $-196 \text{ }^\circ\text{C}$ to $-70 \text{ }^\circ\text{C}$ (in accordance, primarily, with ASTM Standard E-399). At the higher temperatures, where excessive plasticity invalidated direct linear elastic measurements of toughness, values of K_{Ic} were computed from nonlinear elastic J_{Ic} measurements, using the experimental procedures of Sumpter and Turner.³³

Corresponding notched bend fracture tests were performed over a similar temperature range on 19 mm thick, 25 mm wide, four-point bend test pieces with a 45 deg notch, having root radius 0.25 mm. The dimensions of the sample conform to those used in the numerical stress analysis of Griffiths and Owen.³²

To gain insight into the microstructural conditions just prior to failure, double-edge-notched (DEN) four-point bend specimens (with and without fatigue precracks) were tested. The bending moment in such specimens is constant between the two inner loading points. Consequently,

Table I. Composition in Wt Pct of AISI 1008 Steel

| C | Mn | P | S | Si | Fe |
|------|------|------|------|------|---------|
| 0.08 | 0.26 | 0.01 | 0.01 | 0.01 | balance |

Table II. Statistical Parameters, Particle Density, and Grain Diameters

| | S_u (MPa) | S_0 (MPa) | m | N_0 (carbides/ μm^3) | d_g (μm) |
|----|-------------|-------------|------|------------------------------------|-------------------------|
| L3 | 1480 | 2440 | 2.23 | 1.52×10^{-3} | 25 |
| L7 | 1300 | 2840 | 1.65 | 3.71×10^{-4} | 25 |
| H3 | 1480 | 2440 | 2.23 | 1.52×10^{-3} | 45 |
| H7 | 1300 | 2840 | 1.65 | 3.71×10^{-4} | 45 |

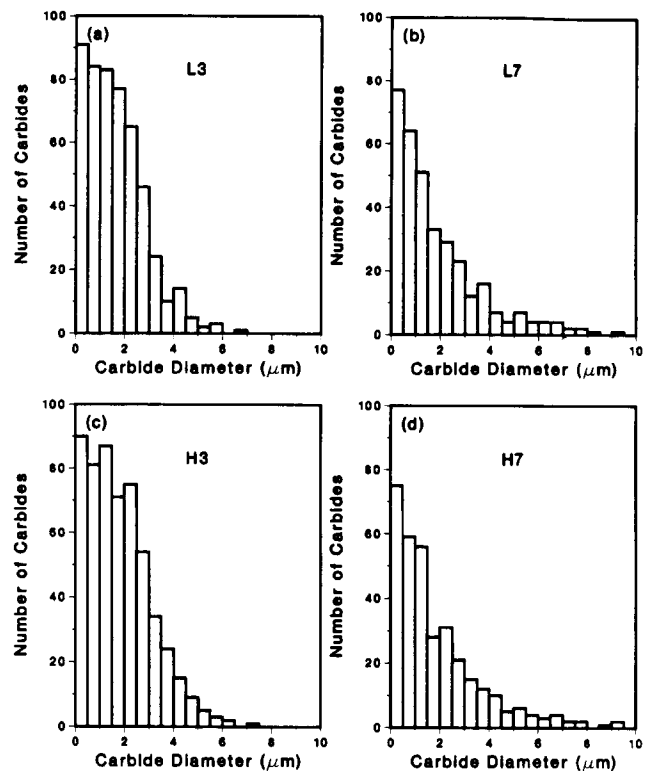


Fig. 5—Particle size distributions for carbides in the four microstructures in AISI 1008 steel following spheroidizing at 700 °C for either 3 or 7 days. L refers to austenitization at 920 °C ($d_g \approx 25 \mu\text{m}$), H to austenitization at 1200 °C ($d_g \approx 45 \mu\text{m}$).

when one notch initiates fracture, conditions at the other (unbroken) notch are representative of those immediately preceding fracture.

V. EXPERIMENTAL RESULTS

A. Mechanical Properties

Statistical parameters for the cumulative particle “strength” distributions for the four microstructures (computed from the size distributions using Eq. [5], with $G_{cf} = 46 \text{ Jm}^{-2}$ ²⁸) are listed in Table II, together with measured values of the grain size, d_g , and number of cracked particles per unit volume, N_0 .

The variation in tensile yield strength, σ_0 , with temperature for the four structures is shown in Figure 6. Other relevant properties are listed in Table III. It is apparent that strength levels are independent of carbide size, but diminish in the coarser-grained microstructures.

Fracture loads and general yield loads (computed from the Von Mises criterion) are shown in Figure 7 for the notched bend tests. At fixed particle size, the fine-grained L3 and L7

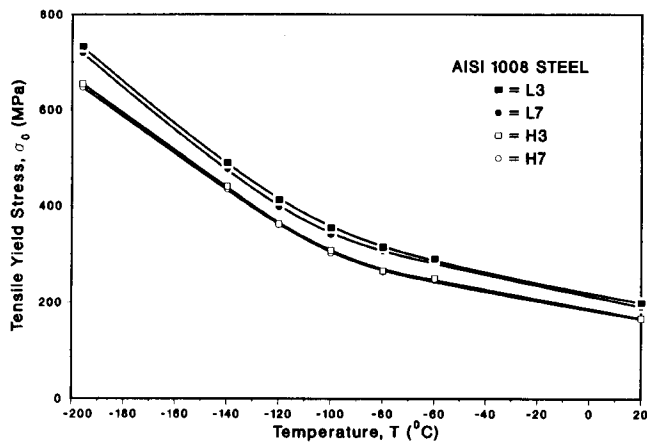


Fig. 6—Experimental measurements of the temperature dependence of the uniaxial tensile yield stress, σ_0 , in the four microstructures.

Table III. Room Temperature Mechanical Properties of AISI 1008 Steel

| Structure | Yield Stress (MPa) | U.T.S. (MPa) | Pct Elong. (on 32 mm) | n |
|-----------|--------------------|--------------|-----------------------|-----|
| L3 | 200 | 320 | 37 | 5 |
| H3 | 167 | 316 | 36 | 5 |
| L7 | 191 | 317 | 37 | 5 |
| H7 | 166 | 316 | 36 | 5 |

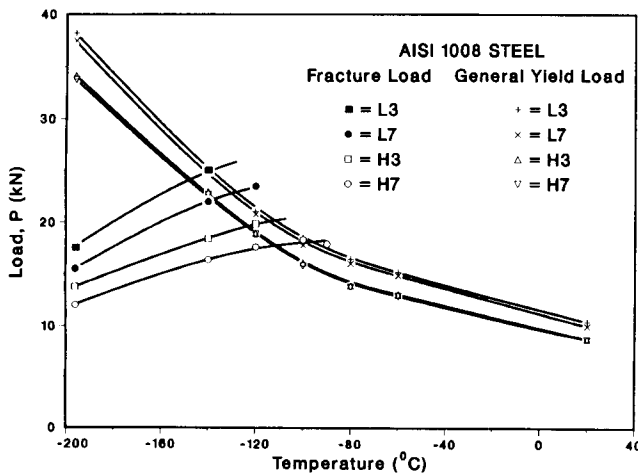


Fig. 7—Experimentally measured variation of the temperature dependence of the load to cause catastrophic cleavage fracture ahead of a rounded notch ($\rho \approx 0.25$ mm) in the four microstructures. Also plotted is the general yield stress, computed from uniaxial data using the von Mises criterion. Note how fine grain sizes and *fine* particle size distributions give the highest toughness.

structures have the highest fracture strength. At fixed grain size, structures with a narrower distribution of finer particles (larger m) have the higher strengths.

Corresponding sharp crack fracture toughness results are plotted in Figure 8. Again, at fixed particle size, the fine-grained microstructures show the highest toughness. However, in contrast to the rounded notch tests, at fixed grain size, structures with a wider distribution of coarser particles have the higher toughness. Thus, microstructures containing *coarse* particles are *tougher* in *sharp crack* tests, whereas

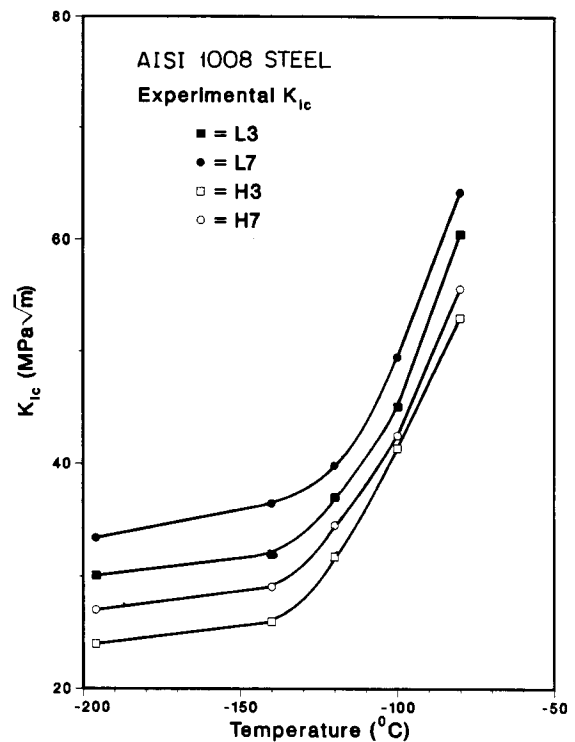


Fig. 8—Experimentally measured variation of the temperature dependence of the (sharp crack) fracture toughness K_{Ic} for cleavage fracture on the lower shelf for the four microstructures. Note how fine grain sizes and *coarse* particle size distributions give the highest toughness.

structures containing *fine* particles are *tougher* in *rounded notch* tests.

B. Fractography

Cracked carbides could not be detected in the vicinity of the unbroken crack or notch tip in DEN specimens at temperatures below -140 °C. However, at -120 °C, numerous carbide microcracks, mostly oriented perpendicular to the applied tensile stress, were observed ahead of the crack tip (Figure 9(a)). No grain-size microcracks were present. Above -100 °C, blunting of the carbide microcracks became prominent (Figure 9(b)). At -90 °C, both microvoids and grain-size microcracks were evident ahead of the crack tip (Figures 10 and 11).

Scanning electron microscopy of a typical cleavage fracture surface, obtained from a sharp crack (Figure 12), reveals the origin and direction of river markings on the cleavage facets. It is apparent that fracture initiated several grains ahead of the tip, most probably at the cavity marked with the arrow. This cavity presumably was the site of the initiating grain-boundary particle, which subsequently become dislodged during the catastrophic fracture process. Additional grain-boundary cavity sites in surrounding grains appear to represent the origin of sets of river markings.

VI. DISCUSSION

Preliminary comparison between theory and experiment is conducted by assuming that the propagation of the cleavage crack across the carbide/ferrite interface is the dominant cleavage mechanism, throughout. The trends in toughness and strength can then be predicted from Eqs. [8] through

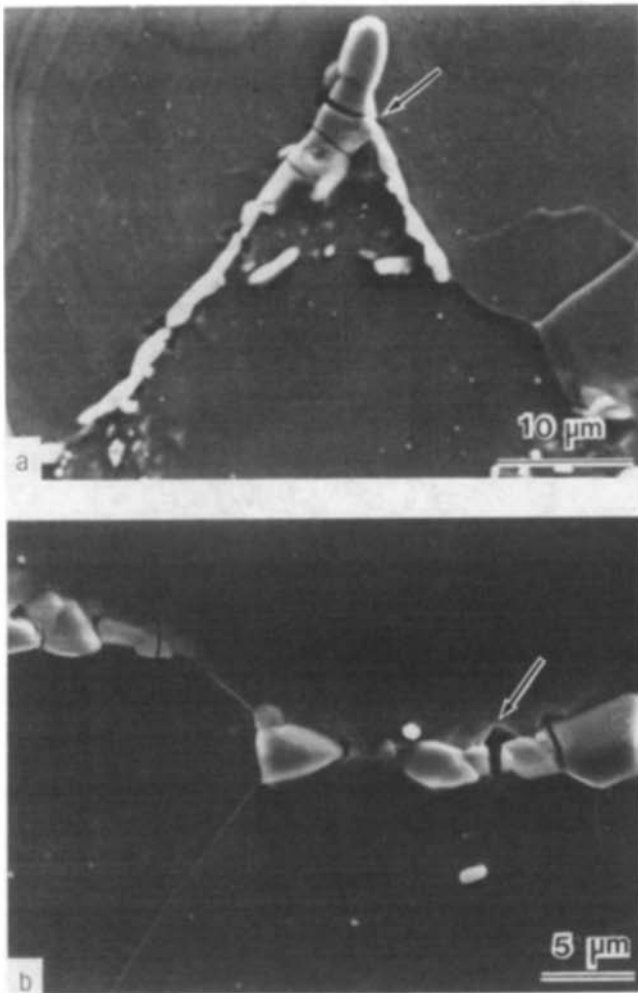


Fig. 9—Scanning electron micrographs of particle microcracks in the L7 microstructure at lower shelf temperatures. Microcracks are formed in grain-boundary carbides several grains ahead of the unbroken fatigue pre-crack (in a DEN specimen), just prior to the onset of catastrophic cleavage fracture at (a) -120°C and (b) -100°C . Note how several carbide microcracks have become blunted at the higher temperature.

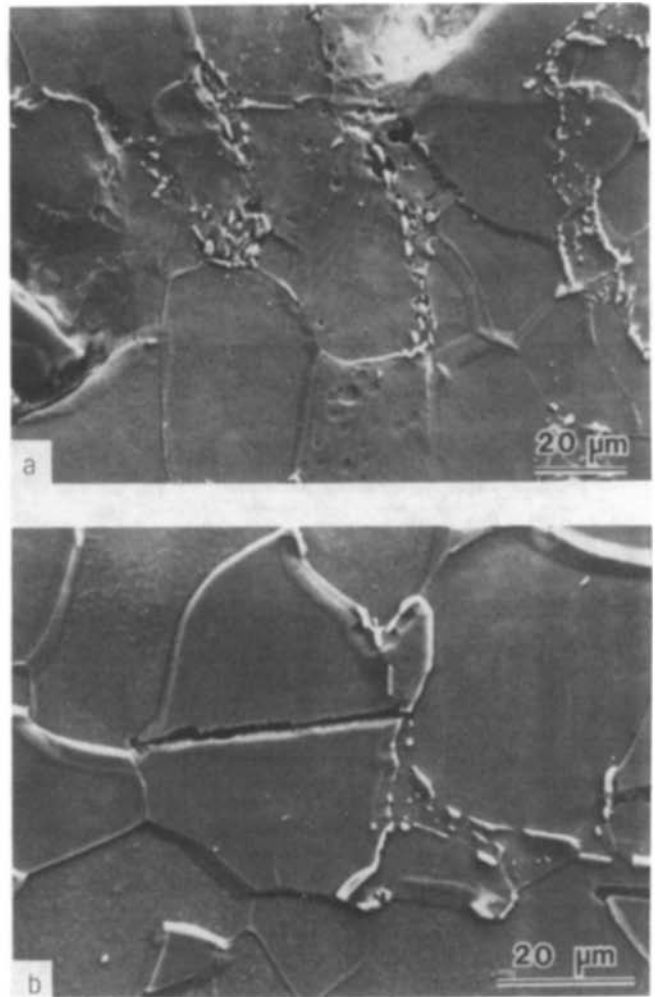


Fig. 11—Enlargement of Figure 10 showing (a) the existence of microvoids formed in the immediate vicinity of the tip of the pre-crack and (b) grain-size microcracks arrested at ferritic grain boundaries, several grains ahead of the tip. Both phenomena are characteristic of cleavage fracture at temperatures in the early ductile/brittle transition range.

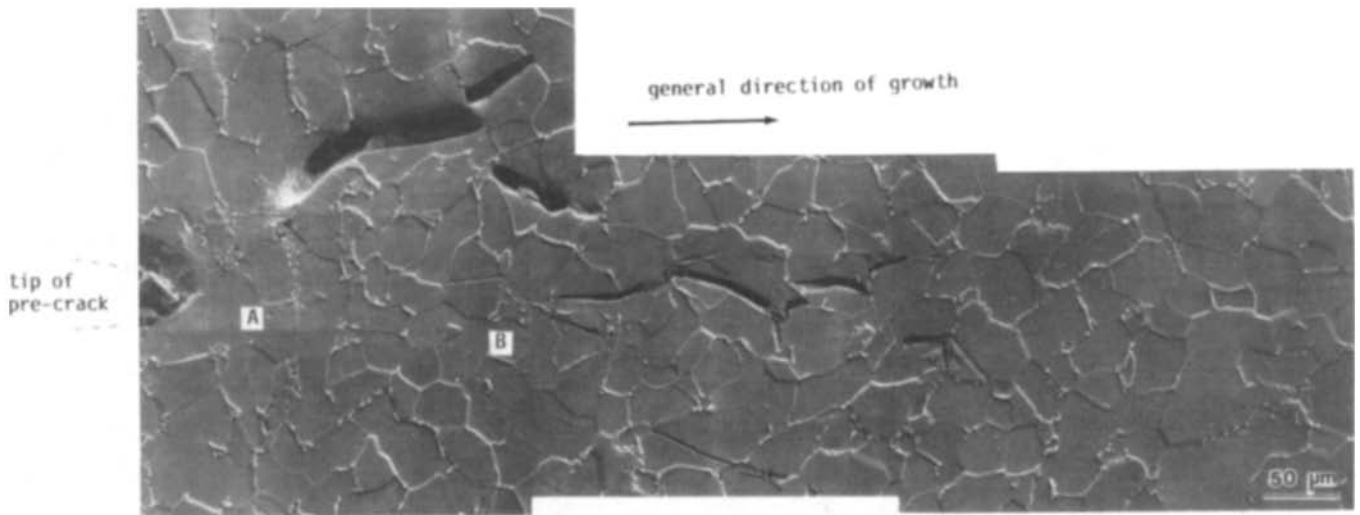


Fig. 10—Scanning electron micrograph of the discontinuous nature of transgranular cleavage cracking at temperatures approaching the early ductile/brittle transition range in H7 microstructure. Metallographic section taken from the center of a fatigue pre-cracked SEN specimen, tested at -90°C (etched in 2 pct nital).

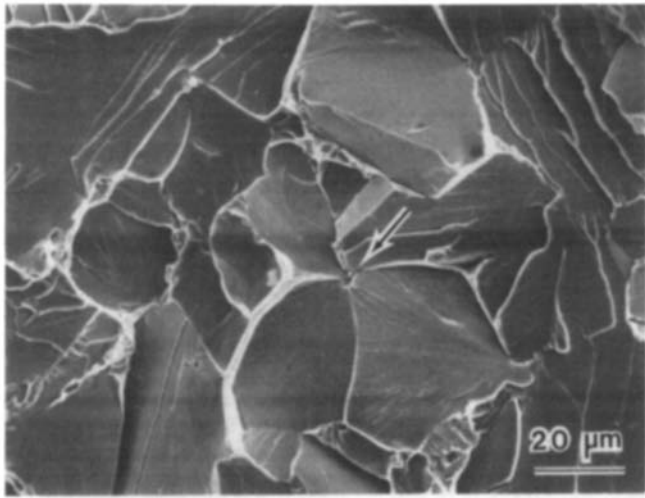


Fig. 12—Scanning electron micrograph of a cleavage fracture surface in a sharp-crack K_{Ic} test at $-120\text{ }^{\circ}\text{C}$ in L7 microstructure, showing possible initiation site at a triple-point grain-boundary carbide ahead of the crack tip. Note how river markings on surrounding cleavage facets point both in the direction of the crack propagation (indicated by arrow) and back toward the tip.¹⁰

[13] by assigning consistent values to the particle eligibility parameter, f , and to the fracture resistance, G_{cf} . Using $f = 0.05$ and $G_{cf} = 46\text{ Jm}^{-2}$, as suggested by previous studies,^{9,10} the predicted variation in K_{Ic} pertinent to the sharp crack tests (Figure 13) and fracture loads for the rounded notch tests (Figure 14) agree quite well with the measured values over the full temperature range.* Based on

*Appreciable crack nucleation controlled or ferrite grain-controlled regimes of cleavage fracture are thus deemed unlikely at lower shelf temperatures in the class of steels used for the present study.

the notion that cleavage fracture is dominated by the carbide particle size distribution, the opposing trends in sharp-crack and rounded-notch toughness with particle size can be rationalized. The probability of failure, and hence the toughness, is related to the number of 'activated' particles having a 'strength' less than the peak stress within the plastic zone, as determined by the product, $N_0[(\sigma - S_u)/S_0]^m$. When the particle distribution is coarsened, the particle density is decreased but the fraction of activated particles is increased. The resultant effect on toughness emerges from the competition between particle spacing, as dictated by particle density, and the particle size, that determines the fraction of activated particles. The relative dominance of these quantities is a function of the magnitude of the local stress. Differing behavior is thus expected for the sharp-crack and rounded-notch (Figure 15). In the case of the rounded-notch, the maximum stress is small (of the order of $2.6\sigma_0$), and the number of activated particles is larger for the coarser carbide L7 microstructure.* Thus, the rounded-

*The accumulated number of activated particles is given by the area under the curve in Figure 15 for strengths less than the appropriate maximum principal stress.

notch toughness is predicted to decrease upon particle coarsening, consistent with the measurements (Figure 14). Conversely, for the sharp notch, the principal stress is much higher (approaching $5\sigma_0$), and the number of activated

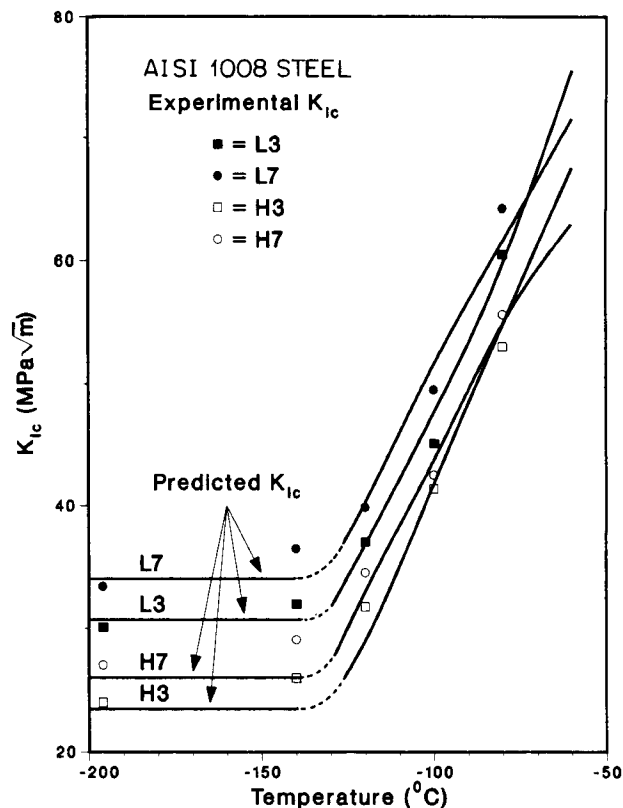


Fig. 13—Comparison of the experimental and predicted (Eq. [11]) variation of the temperature dependence of the plane strain fracture toughness, K_{Ic} , for catastrophic cleavage fracture. Predictions for lowest temperatures are based on the linear elastic solution (Eq. [11a]), whereas at higher temperatures the nonlinear elastic solution (Eq. [11b]) is used. Results indicate that increased (sharp-crack) toughness is achieved with fine grain size and coarse particle distributions.

carbides is now larger for the finer carbide L3 microstructure (Figure 15(a)). The sharp-crack toughness at the lower temperatures ($\lesssim -100\text{ }^{\circ}\text{C}$) is thus predicted to increase upon particle coarsening, again consistent with the K_{Ic} results (Figure 13). With further coarsening of the particle distribution (the L30 structure, Figure 16), both the sharp-crack and rounded-notch toughness decrease. Similarly, as temperature is increased, the decrease in stress due to the lower yield strength causes the particle coarsening to have the same effect on the sharp-crack toughness as on the rounded-notch toughness (Figure 17), resulting in the crossover in predicted K_{Ic} at higher temperatures, above $-100\text{ }^{\circ}\text{C}$ (Figure 13).

Increasing the grain size results in a decrease in the yield strength σ_0 , which increases toughness. Consequently, by incorporating the Hall-Petch relationship,^{34,35} an optimum grain size for maximum toughness can be predicted,

$$d_g^* = \left[\frac{k_y(n-2)}{\sigma_i} \right]^2 \quad [14]$$

where σ_i is the lattice friction stress and k_y is the slope of the σ_0 vs $d_g^{-1/2}$ Hall-Petch plot. For temperatures on the lower toughness shelf, calculated values of d_g^* values are ~ 2 to $14\text{ }\mu\text{m}$, much finer than the grain sizes employed in the present study. The model thus predicts a decreasing toughness with increasing grain size (at fixed particle size and volume fraction), for both sharp-cracks and rounded-

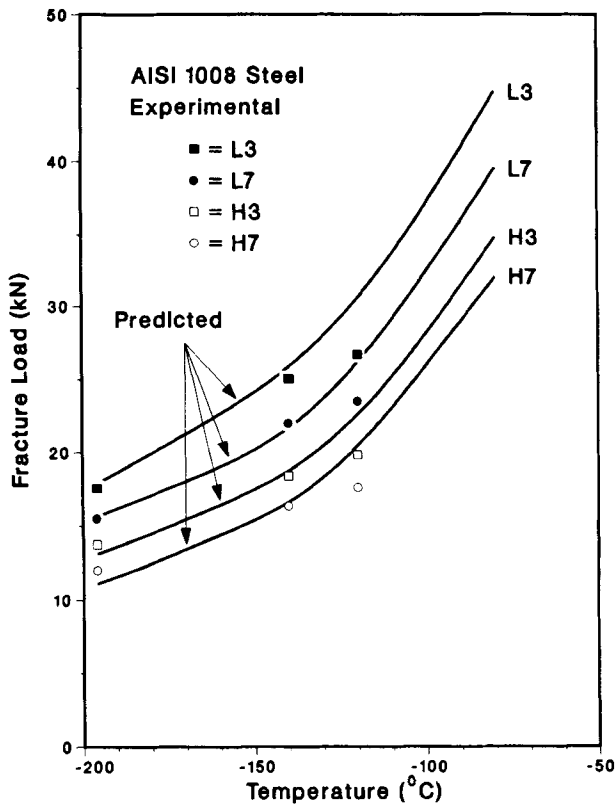


Fig. 14—Comparison of the experimental and predicted (Eqs. [12],[13]) variation of the temperature dependence of the load required for catastrophic cleavage fracture ahead of a rounded notch at lower shelf temperatures. Results indicate that increased (rounded-notch) toughness is achieved with fine grain size and fine particle size distributions.

notches, consistent with the experimental results (Figures 13 and 14).

VII. CONCLUDING REMARKS

By varying independently the grain and particle size in a low carbon steel having a ferritic/grain-boundary carbide microstructure, it is shown that whereas the notch toughness is increased, the sharp-crack toughness is decreased by refining the carbide particle size, at fixed grain size. However, grain size refinement at fixed carbide particle size increases both the notch and sharp-crack toughness. The effects of carbide particle size and grain size on the low temperature notch and sharp-crack toughness are predicted correctly by a statistical model, wherein crack extension across the carbide/ferrite interface is the critical step in cleavage fracture. Physically, the effect is related to the significantly higher stresses generated ahead of a sharp crack, and the resultant influence on the number of particles activated within the plastic zone.

The present study has emphasized cleavage fracture at temperatures wherein the critical step involves the propagation of a particle microcrack into the surrounding grains. However, at higher temperatures, following the transition to ferrite grain controlled microcracking (Figure 3), the dependence of toughness on grain size would differ from that described in the present article. Moreover, the grain-size microcracks probably interact and alternative stochastic models (*e.g.*, Reference 36) would be needed to predict the trends in toughness. Additionally, crack bridging by unbroken ligaments is likely to be important at the higher temperatures, in the transition region.³⁷

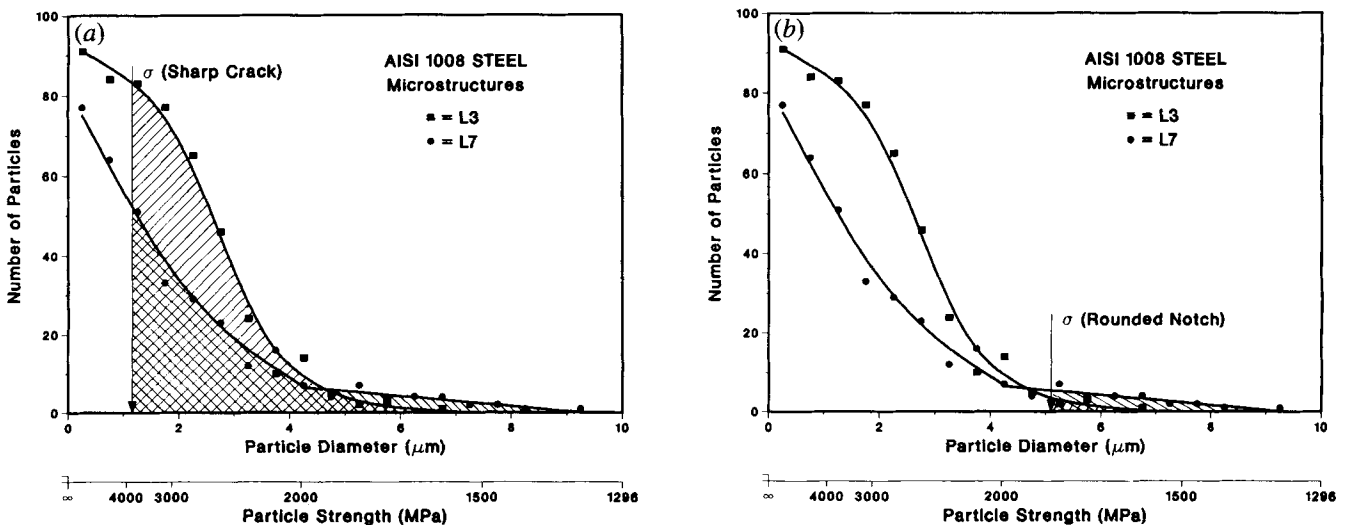


Fig. 15—Total number of carbide particles in the plastic zone, as a function of particle diameter and strength, for the fine and coarse particle distributions (L3 and L7 structures). The number of activated carbides, which is inversely proportional to toughness, is given by the accumulated number of particles with strengths less than the maximum principal stress σ ahead of (a) a sharp crack and (b) a rounded notch at -196°C . Note that for sharp-crack toughness, the coarse particle distribution yields the smaller number of activated carbides and hence the larger toughness, whereas the reverse is true for the rounded notch.

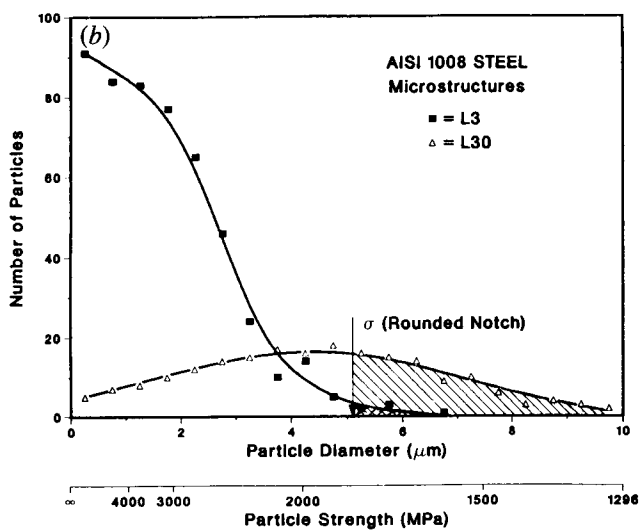
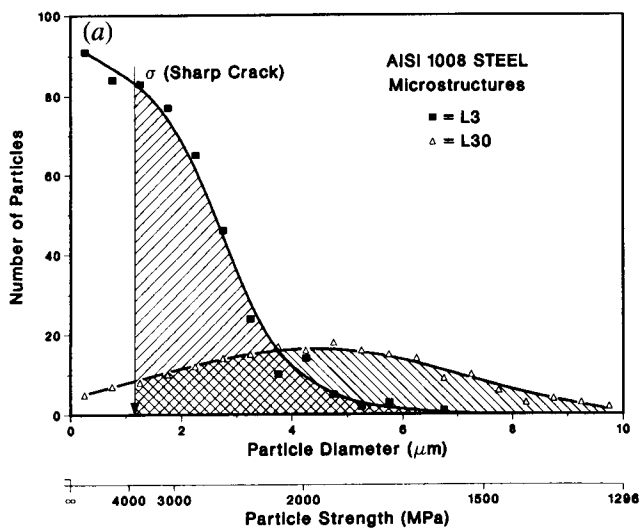


Fig. 16—Total number of carbides within the plastic zone for fine (L3) and very coarse (L30) particle size distributions, showing how the number of activated carbides is increased, and the toughness is decreased, for both (a) sharp cracks and (b) rounded notches at -196°C , with excessive coarsening of the particle distribution.

VIII. SUMMARY AND CONCLUSIONS

A weakest link statistical model for transgranular cleavage fracture has been applied to the problem of the independent roles of grain size and particle size in influencing brittle fracture in single phase microstructures containing a known distribution of noninteracting particles acting as potential crack nuclei. The model, which is based on the extension of a particle microcrack into the matrix, is shown to predict accurately the cleavage fracture load ahead of a rounded notch and the sharp-crack fracture toughness, K_{Ic} , as a function of temperature on the lower toughness shelf.

By varying independently the grain and particle size in a low carbon steel, with ferritic/grain-boundary carbide microstructure, it is shown experimentally that whereas the rounded-notch toughness is *increased*, the sharp-crack toughness is *decreased* by refining the particle size distribution (at fixed grain size). Corresponding refinement in grain size (at fixed particle size), conversely, increases both the rounded-notch and sharp-crack toughness. This con-

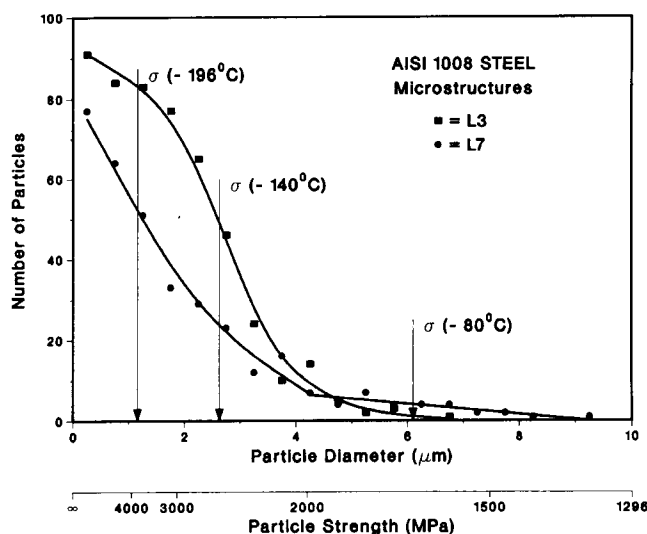


Fig. 17—Total number of carbides within the plastic zone for fine (L3) and coarse (L7) particle distributions, showing that at higher temperatures (above $\sim -80^{\circ}\text{C}$), the reduction in peak local tensile stress ahead of a sharp crack results in behavior similar to that of the rounded notch, *i.e.*, to a larger number of activated carbides and hence a lower toughness with increasing particle size distribution.

flicting effect of particle and grain size on the low temperature toughness is shown to be predicted correctly by the model, and is physically related to the higher stresses and differing number of activated particles generated ahead of a sharp crack.

NOMENCLATURE

| | |
|------------------|---|
| a | crack, or notch, length |
| \dot{a} | crack velocity |
| b | characteristic dimension along crack front |
| c | terminal velocity of sound wave in the solid |
| d_g | average grain diameter |
| d_g^* | optimum grain size for maximum toughness |
| d_p | diameter of cracked particle |
| D_1, D_2 | functions of $\bar{\epsilon}_t/\epsilon_0$ and r/ρ , respectively, in Eq. [13] |
| E | Young's modulus |
| f | "eligibility" factor in Eq. [9] |
| $g(S) dS$ | elemental strength distribution of particles |
| G_{cf}, G_{ff} | dynamic strain energy release rates for crack growth through particle/matrix and matrix/matrix interfaces, respectively |
| I_n | dimensionless parameter in HRR singular solution |
| J | path-independent integral; amplitude of HRR singular field |
| J_{Ic} | crack initiation fracture toughness ($= K_{Ic}^2/E$) |
| k_y | slope of the Hall-Petch σ_0 vs $d_g^{-1/2}$ plot |
| K_I | stress intensity factor (Mode I) |
| K_{Ic} | plane strain fracture toughness |
| m | shape factor in Weibull formulation |
| n | work hardening exponent ($1 < n < \infty$) |
| N_0 | number of particles per unit volume (particle density) |
| r, θ | polar coordinates, centered at crack tip or notch root |
| r_N^* | most probable site for crack initiation |

| | |
|--------------------------------|--|
| r_y | plastic zone size |
| r_f^* | characteristic distance from tip (at $K_I = K_{Ic}$) |
| s | function of S_u and σ_0 in Eq. [12] |
| S | fracture "strength" of particle |
| S_0 | scale parameter in Weibull formulation |
| S_u | fracture "strength" of largest observable particle |
| $\delta V, V$ | elemental and total active zone volume, respectively |
| δ | crack tip opening displacement |
| $\bar{\epsilon}_T$ | equivalent strain at notch root |
| ζ | factor describing boundary of slip-line field |
| η | function of m , S , and S_u in Eq. [11] |
| λ | coefficient in Eq. [2], of order 2 |
| ν | Poisson's ratio |
| ξ | function of n , $\bar{\sigma}$, ν , and I_n in Eq. [11] |
| ρ | root radius of notch |
| σ | local stress within plastic zone |
| $\hat{\sigma}$ | peak stress within plastic zone |
| $\bar{\sigma}, \bar{\epsilon}$ | equivalent stress and strain, respectively |
| σ_c | critical stress to nucleate crack in particle |
| σ_f^* | cleavage fracture stress |
| σ_i | lattice friction stress in Hall-Petch relationship |
| $\tilde{\sigma}_{ij}$ | function in HRR crack tip field singular solution |
| σ_m | mean (or hydrostatic) stress |
| σ_0, ϵ_0 | flow (or yield) stress and strain, respectively |
| σ_{11} | tensile stress |
| Σ | fracture "strength" of matrix grain |
| $\delta\phi, \Phi$ | elemental and total failure probabilities |

ACKNOWLEDGMENTS

This work was supported by the Director, Office of Energy Research, Office of Basic Energy Sciences, Materials Science Division of the United States Department of Energy under Contract No. DE-AC03-76SF00098. The authors thank Ms. Madeleine Penton for her assistance in preparing the manuscript.

REFERENCES

1. C. Zener: in *Fracturing of Metals*, American Society for Metals, Cleveland, OH, 1948, p. 3.
2. A. N. Stroh: *Proc. Royal Soc.*, 1954, vol. A223, p. 404.
3. A. H. Cottrell: *Trans. AIME*, 1958, vol. 212, p. 192.
4. W. H. Buckner: *Weld. J. Res. Suppl.*, 1950, vol. 29, p. 467-S.
5. C. J. McMahon and M. Cohen: *Acta Metall.*, 1965, vol. 13, pp. 591-604.
6. E. Smith: in *Proceedings of Conf. on Physical Basis of Yield and Fracture*, Institute of Physics, Oxford, U.K., 1966, pp. 36-45.
7. D. Curry and J. F. Knott: *Met. Sci.*, 1978, vol. 12, pp. 511-14.
8. M. Holzmann and J. Man: *J. Iron & Steel Inst.*, 1971, vol. 209, pp. 836-38.
9. Tsann Lin, A. G. Evans, and R. O. Ritchie: *J. Mech. Phys. Solids*, 1986, vol. 34, pp. 477-97.
10. Tsann Lin, A. G. Evans, and R. O. Ritchie: *Acta Metall.*, 1986, vol. 34, pp. 2205-16.
11. A. R. Rosenfield, D. K. Shetty, and A. J. Skidmore: *Metall. Trans. A*, 1983, vol. 14A, p. 1934.
12. J. F. Knott: *Fundamentals of Fracture Mechanics*, Butterworths, London, U.K., 1973.
13. T. R. Wilshaw, C. A. Rau, and A. S. Tetelman: *Eng. Fract. Mech.*, 1968, vol. 1, pp. 191-211.
14. J. F. Knott: *J. Iron & Steel Inst.*, 1966, vol. 204, pp. 104-11.
15. R. O. Ritchie, J. F. Knott, and J. R. Rice: *J. Mech. Phys. Solids*, 1973, vol. 21, pp. 395-410.
16. D. Curry and J. F. Knott: *Met. Sci.*, 1979, vol. 13, pp. 341-45.
17. F. M. Beremin: *Metall. Trans. A*, 1983, vol. 14A, pp. 2277-87.
18. K. Wallin, T. Saario, and K. Törrönen: *Met. Sci.*, 1984, vol. 18, pp. 13-16.
19. A. G. Evans: *Metall. Trans. A*, 1983, vol. 14A, pp. 1349-55.
20. Chun-xiao Hou, Qi-gong Cai, Yi Su, and Xiu-yuan Zheng: in *Advances in Fracture Research '84*, Proc. Sixth Int. Conf. on Fracture, New Delhi, India, Dec. 1984, S. R. Valluri, ed., Pergamon Press, Oxford, U.K., 1984, vol. 2, pp. 1415-22.
21. A. S. Argon, J. Im, and R. Safoglu: *Metall. Trans. A*, 1975, vol. 6A, pp. 825-51.
22. J. W. Hutchinson: *J. Mech. Phys. Solids*, 1968, vol. 16, pp. 13-31.
23. J. R. Rice and G. R. Rosengren: *J. Mech. Phys. Solids*, 1968, vol. 16, pp. 1-12.
24. C. F. Shih: Division of Engineering, Brown University Report No. MRL E-147, Providence, RI, June 1983.
25. M. Cohen and M. R. Vukcevic: in *Physics of Strength and Plasticity*, A. S. Argon, ed., M.I.T. Press, Cambridge, MA, 1969, pp. 295-305.
26. A. G. Evans, M. Ruhle, and M. Turwitt: *J. de Physique*, 1985, vol. 46, p. 613.
27. J. W. Hutchinson and L. B. Freund: *J. Mech. Phys. Solids*, 1985, vol. 33, pp. 169-92.
28. W. W. Gerberich and E. Kurman: *Scripta Metall.*, 1985, vol. 19, pp. 295-98.
29. J. R. Matthews, W. Shack, and F. A. McClintock: *J. Amer. Cer. Soc.*, 1976, vol. 59, pp. 305-08.
30. W. Weibull: *Ingen. Vetenskap. Akad. Handl.*, 1938, vol. 151, pp. 1-45.
31. R. Hill: *The Mathematical Theory of Plasticity*, Clarendon Press, Oxford, U.K., 1950.
32. J. R. Griffiths and W. S. Owen: *J. Mech. Phys. Solids*, 1971, vol. 19, pp. 419-31.
33. J. D. G. Sumpter and C. E. Turner: in *Cracks and Fracture*, ASTM STP 601, American Society for Testing and Materials, Philadelphia, PA, 1976, pp. 3-18.
34. E. O. Hall: *Proc. Phys. Soc.*, 1951, vol. 64B, p. 747.
35. N. J. Petch: *J. Iron & Steel Inst.*, 1953, vol. 173, p. 25.
36. W. W. Gerberich: in *Fracture Mechanics: 18th Symposium*, ASTM STP, R. P. Reed and D. T. Read, eds., American Society for Testing and Materials, Philadelphia, PA, in press.
37. A. R. Rosenfield and B. S. Majumdar: in *Local Approach to Fracture*, Proc. Intl. Seminar, Moret-sur-Loing, France, June 1986, in press.